

Article

Properties Evolution of Some Hydraulic Mortars Incorporating Graphene Oxides

Popa Dorin ¹, Prodan Doina ^{2,*}, Varvara Simona ¹, Popa Maria ³, Cuc Stanca ^{2,*}, Sarosi Codruta ²,
Moldovan Marioara ², Ivan Raluca ³ and Ene Razvan ^{4,5}

- ¹ Faculty of Exact Sciences and Engineering, “1 Decembrie 1918” University of Alba Iulia, 510009 Alba Iulia, Romania; dpopa@uab.ro (P.D.); svarvara@uab.ro (V.S.)
- ² “Raluca Ripan” Institute of Research in Chemistry, “Babes Bolyai” University, 400294 Cluj-Napoca, Romania; codruta.sarosi@ubbcluj.ro (S.C.); marioara.moldovan@ubbcluj.ro (M.M.)
- ³ Faculty of Economic Sciences, “1 Decembrie 1918” University of Alba Iulia, 510009 Alba Iulia, Romania; mpopa@uab.ro (P.M.); raluca.ivan@uab.ro (I.R.)
- ⁴ 14 Department of Orthopedics, Anesthesia and Intensive Care, University of Medicine and Pharmacy “Carol Davila”, 020021 Bucharest, Romania; razvan77ene@yahoo.com
- ⁵ Orthopedics and Traumatology Department, Bucharest Emergency University Hospital, 020021 Bucharest, Romania
- * Correspondence: doina.prodan@ubbcluj.ro (P.D.); stanca.boboia@ubbcluj.ro (C.S.); Tel.: +40-0724254336 (P.D.); +40-0757939232 (C.S.)

Abstract: In this experimental study, the mechanical and adhesion properties of several hydraulic lime mortars incorporating graphene oxide (GO)-based nanomaterials were evaluated. Four different composite mortar samples were prepared by adding different percentages of GO-based powders (functionalized), i.e., 1 wt.% GO, 5 wt.% GO, 5wt.% GO-Ag-GO-Fly ash, and 5 wt.% GO-ZnO-GO-TiO₂ into the reference mortar sample. The mortar specimens were analyzed through mechanical tests, FT-IR, and SEM. The behavior of selected mortars exposed to chemical attacks was also investigated. The results indicate that the addition of the functionalized GO-based powders leads to a significant improvement in the mortar’s adhesion to the brick substrate (up to 80%) compared to the reference sample, especially in the case of the hydraulic lime mortar incorporating the mixture of GO-Ag and GO-Fly ash, which also showed good resistance to chemical attacks.

Keywords: hydraulic mortars; graphene oxide; mechanical properties



Citation: Dorin, P.; Doina, P.; Simona, V.; Maria, P.; Stanca, C.; Codruta, S.; Marioara, M.; Raluca, I.; Razvan, E. Properties Evolution of Some Hydraulic Mortars Incorporating Graphene Oxides. *Buildings* **2022**, *12*, 864. <https://doi.org/10.3390/buildings12060864>

Academic Editors: Cesare Oliviero Rossi, Pietro Calandra, Paolino Caputo, Bagdat Teltayev, Valeria Loise and Michele Porto

Received: 13 May 2022

Accepted: 16 June 2022

Published: 20 June 2022

Publisher’s Note: MDPI stays neutral with regard to jurisdictional claims in published maps and institutional affiliations.



Copyright: © 2022 by the authors. Licensee MDPI, Basel, Switzerland. This article is an open access article distributed under the terms and conditions of the Creative Commons Attribution (CC BY) license (<https://creativecommons.org/licenses/by/4.0/>).

1. Introduction

It is known that the characteristics of the mortars used in cultural and historical building conservation and restoration works can be modelled by controlling several factors, such as the nature and the ratio of the binder and the aggregate, the addition of various additives, etc. [1,2].

During restoration works on a historical building, it is crucial to ensure the materials’ compatibility, not only in terms of chemical and physical characteristics, but also regarding the level of mechanical strength [3].

In the last decade, Natural Hydraulic Lime (NHL) mortars have been extensively used for the restoration of historical structures, due to their enhanced compatibility with historical materials [4]. However, when choosing an NHL, it is not always the best solution to use the hardest lime. For instance, in the case of historical masonry, the mechanical strength could be less important than the chemical and physical compatibility of the materials [4]. An NHL 3.5 used for plastering will give the layer its sweating properties, allowing the control of the relative humidity in indoor spaces. Furthermore, due to its low modulus of elasticity, NHL 3.5 has the ability to work with the natural bricks in the masonry, compensating for the effects of thermal expansion and, thus ensuring greater

durability [5]. However, the environmental conditions and degree of mortar exposure to atmospheric agents should be also considered.

Recently, it was found that various nanomaterials, such as nano-TiO₂ [6,7] and graphene [8,9] could be successfully used to improve the mechanical properties and durability of the mortars [10–12]. Nano-TiO₂ has been also proved an excellent photocatalytic material that imparts biocidal, self-cleaning, and smog-abating functionalities when added to cement-based materials [13,14].

Graphene oxide (GO) nanofoils, an oxidized derivative of graphene, present an extremely large, specific surface area, excellent mechanical properties, and thermal conductivity, while their surface contains a large number of active groups containing oxygen, such as hydroxyl, carboxyl, and epoxy groups [15]. Recent studies proved that graphene oxide (GO) nanofoils are highly effective for improving the mechanical properties of cement-based materials [16–20].

Special attention has also been paid to the development of nanocomposite materials that combine GO with different nanoparticles, such as Ag, Ag/ZnO, TiO₂, SiO₂, ZnO, etc. For instance, silver-doped graphene oxide materials have favorable properties of low strength, good dispersion, and improved mechanical strength [21]. El-Shafai et al. [22] also reported that the GO sheets functionalized with Ag/ZnO could improve the antibacterial and antifungal effect of the materials into which they are introduced [22], by inhibiting the pathogens' growth. Likewise, the doped ZnO powders containing small amounts of Ag revealed good antimicrobial properties, which allowed their application as pigments for indoor and outdoor painting [23].

Fly ash is a by-product of coal-fired thermal power plants that is used as fine aggregate (filler) in mortars, leading to considerable improvements in their strength [24]. Fly ash is made of mud-sized particles, which are generally spherical, usually between 10 and 100 microns in size. These small spheres of glass improve the fluidity and workability of the fresh mortar. Finesse is another important property that contributes to the pozzolanic reactivity of the fly ash [25]. Oltulu et al. [26] showed that the addition of nano-SiO₂, nano-Al₂O₃ and nano-Fe₂O₃ powders into the cement mortar containing fly ash improved the mechanical and physical properties of the mortars by increasing their pozzolanic activity.

The aim of this study is to obtain four mortar variants, with additives based on graphene oxide/mixtures of functionalized graphene oxides, intended for the restoration of old buildings (churches, historic buildings), in order to improve their adhesion to the original masonry components which have deteriorated over time and must be restored. There are situations in which the use of a cement mortar has created problems, proving to be ineffective. Historical mortars are usually weak mortars that crumble to the touch. It is known that lime hydraulic mortars are more permeable to water vapor and also that the mortars with lower compressive strengths are more susceptible to higher permeability rates. The aim is for these graphene mortars to ensure good adhesion to defects or mortar joints that need to be repaired, ensuring adequate compatibility with the original mortar. Hydraulic lime mortars (NHL) harden over a much longer period of time than cement mortars, therefore it is recommended that the restored site be kept dry until it has hardened. The study also focused on determining the mechanical properties, looking at how the addition of graphene oxide additives can influence them in a positive or negative way. The obvious aim is to slightly improve these properties compared to the reference material, but without increasing them too much, so that compatibility with the original mortars can be maintained. The newly experimental mortars were characterized by mechanical tests, Fourier transform infrared spectroscopy (FT-IR), and scanning electron microscopy (SEM). The evaluated physical properties of the mortars include the compressive and flexural strength, as well as their adhesion to the brick substrate. The microstructural changes of the selected composite mortars exposed to chemical attacks were also studied.

2. Materials and Methods

2.1. Materials

The basic mixture of the reference mortar (M) was prepared using a commercial natural hydraulic lime (NHL 3.5) with a 2% dependence on methacholine (Metastar 402 from Imerys Minerals) as the binder (Table 1). It was supplied by Calix Blanca, Italcementi, Bologna, Italy. The NHL 3.5 natural hydraulic lime is suitable for preparing mortars used for various applications, including masonry, rendering, plastering or interior and exterior finishing. The mechanical characteristics, porosity, and low salt content of NHL 3.5 ensure its compatibility with traditional construction materials (i.e., brick and stone masonry, earth, and vault constructions, etc.), which makes it suitable for conservation, restoration, and maintenance works for cultural and historical buildings and monuments.

Table 1. The recipe for mortar preparation.

Mortar Code	NHL 3.5/Sand *	Water/NHL 3.5 [wt%]	Graphene Oxide Powders/NHL 3.5 [wt%]				
			GO	GO-Ag	GO-Fly Ash	GO-ZnO	GO-TiO ₂
M	1/2.5	1.05	0	0	0	0	0
M-GO-1%	1/2.5	1.05	1	0	0	0	0
M-GO-5%	1/2.5	1.05	5	0	0	0	0
M-GO-Ag-GO-Fly ash	1/2.5	1.05	0	2.5	2.5	0	0
M-GO-ZnO-GO-TiO ₂	1/2.5	1.05	0	0	0	2.5	2.5

* Construction sand 0.7–1 mm (AdePalast).

2.2. Characterization Techniques

2.2.1. Fourier Transform Infrared Spectrometry (FT-IR)

FTIR analysis was performed in order to determine if there were changes in the absorption bands with the introduction of graphene oxide additives in the composition of the mortars, or depending on their concentration. It is also possible to make a comparison of the experimental mortars with those used in the original plaster, by inputting evidence of the absorption peaks, attributed to the vibrations from the specific functional groups of the components.

The ATR-FTIR spectra of the hardened mortar samples were recorded using an FTIR spectrophotometer (Jasco Europe srl, Cremella, Italy) equipped with a total attenuated reflectance (ATR) attachment with horizontal ZnSe crystal (Jasco PRO400S). The FTIR spectra were measured with a resolution of 4 cm⁻¹, in the spectral range of 4000–500 cm⁻¹, and the scans were repeated 100 times.

2.2.2. Mechanical Tests

The durability of mortar is a significant parameter to ensure that successful restoration ensues and should be assessed either through laboratory studies [27] or in-situ tests [28].

In order to better identify the differences between the five types of mortars tested, the results were subjected to an Anova one-way statistical analysis, using Origin2019b graphing and analysis (OriginLab). The Tukey test was also used to better understand the differences between the five mortars. The null hypothesis is that the means of all levels are equal. The results were considered significant for $p \leq 0.05$. The study groups (Table 1) are the five different mortar recipes, with comparisons being made between all of them for each mechanical test, and each group being represented by $n = 20$ results.

The preparation of the samples was subjected to the flexural and compressive strength of the hardened mortars and was carried out in accordance with SR EN 1015-11:2002 [29].

The compressive strength tests of all the mortar mixes were performed on 40 mm × 40 mm × 40 mm cubical mortar specimens after 28 days of curing. The specimens were compressed using a Lloyd Instruments mechanical testing machine (Ametek LR5K Plus

Twin Column Bench Mounted) using the BS EN 1607-1997 test [30]. The maximum load cell was 5 kN, and the load on the samples was applied at a speed of 0.5 mm/min and a uniform force of 2000 N. For each type of recipe, 20 tests were recorded.

The flexural strength tests were performed on 160 mm × 40 mm × 40 mm mortar specimens, measured using three-point bending tests on three beams. The samples were subjected to a force up to fracture using the Lloyd Instruments mechanical testing machine at a loading rate of 50 N/s, using the ASTM C 348-14 [31] test. For each type of recipe, 20 tests were recorded.

The determination of the adhesive strength of the tested mortars was performed according to SR EN 1015-12: 2001 [32], using tensile pellets attached (5 cm in diameter) to the investigated mortars with a universal adhesive (Bison Epoxy, 5 min—2 component epoxy adhesive). A 10 cm brick was used as a base surface for the adhesive strength tests. The mortars were applied in a 20 mm layer on solid wet bricks, which were kept in a vertical position during the application. The adhesion strengths were estimated by the pull-off method, at a temperature of 25 °C, 55% humidity and a peel speed of 10 mm/min, using the Lloyd Instruments Mechanical Testing Machine. For each type of mortar recipe, 20 substrate adhesion tests were recorded.

2.2.3. Scanning Electron Microscopy (SEM)

For SEM investigations, the 28-day cured mortar samples taken from fractured mortar specimens after mechanical testing were used. The morphological and structural characterization of the fragments' surfaces was performed using an Inspect S electron microscope (FEI Hillsboro, OR, USA) at low vacuum, with an acceleration voltage of 30 kV and magnifications of 1000×, 5000×, 10000×.

2.2.4. Experimental Studies for the Evaluation of Mortars Exposed to Corrosive Attacks

In order to evaluate the behavior of the mortars in various external environmental conditions, chemical attacks were applied on selected mortar samples, i.e., the reference mortar (M) and the mortar sample containing GO-Ag and GO-Fly ash (M-GO-Ag-GO-Fly ash). Three different substances that simulate acidic rain and external corrosive factors were used for chemical attacks, as follows: rainwater, acetic acid, and a mixture of strong acids.

The morphological changes on the surface of the mortars following chemical attack at different pH values were investigated using SEM. The initial structures of the selected mortars were also analyzed.

For this study, mortar specimens of 40 × 40 × 80 mm dimension were prepared and cured for 28 days, at room temperature. One surface of the specimens was exposed to chemical attack, while the rest of the surface was sealed with epoxy resin.

The corrosive solutions were: (a) rainwater, pH = 6 (RW); (b) a solution of acetic acid (1:5) with a pH-value of 3.5. Several drops of ammonia were used for the pH adjustment (AA); (c) a mixture of sulphuric acid and nitric acid at pH = 2 (18 cm³ distilled water + H₂SO₄ 98% + 2 cm³ HNO₃ 65% + ammonia as acidity regulator, until pH = 2 (SNA).

The samples were stored at room temperature for 7 days. Each day, 2 mm of the free surfaces were immersed in the corrosive solutions for 30 min and then analyzed using SEM.

3. Results and Discussions

3.1. Fourier Transform Infrared Spectrometry (FT-IR)

Figure 1 shows the FT-IR spectra of the reference mortar sample (M) and the newly prepared mortar samples containing GO (M-GO-1% and M-GO-5%) and GO functionalized with Ag, Fly ash, ZnO and TiO₂ (M-GO-Ag-GO-Fly ash and M-GO-ZnO-GO-TiO₂), in the wavenumber range of 4000–500 cm⁻¹. The wavelengths of the most important absorption peaks from Figure 1 are illustrated in Table 2.

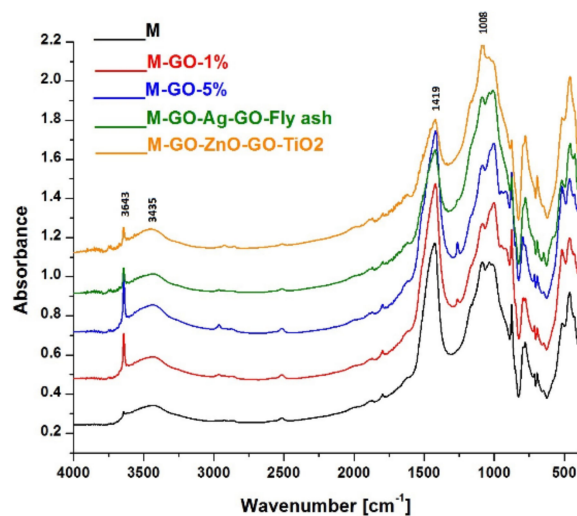


Figure 1. FT-IR spectra of the investigated mortars.

Table 2. The main maxima identified in the FT-IR spectra of the investigated mortars.

Mortar Sample	FT-IR Maximum [cm^{-1}]			
M	3644	3422	1423	1083
M-GO-1%	3642	3427	1419	1000
M-GO-5%	3642	3446	1419	1006
M-GO-Ag-GO-Fly ash	3643	3436	1419	1008
M-GO-ZnO-GO-TiO ₂	3643	3435	1419	1008

As seen in Figure 1, the FT-IR spectra of all graphene-containing mortars are similar to that of the reference sample. Four distinct groups of absorption bands can be identified in the ranges of $3642\text{--}3644\text{ cm}^{-1}$, $3422\text{--}3446\text{ cm}^{-1}$, $1419\text{--}1423\text{ cm}^{-1}$ and $1000\text{--}1083\text{ cm}^{-1}$. An absorption peak at around 3640 cm^{-1} is noticeable in all the spectra from Figure 1. It could be attributed to the stretching vibrations of the hydroxyl group from $\text{Ca}(\text{OH})_2$. The wide band at 3436 cm^{-1} corresponds to the stretching vibrations of the O-H bond, which can also be attributed to the oxygen groups found both on the surface and at the edge of the GO sheets [8,33]. The third band could be assigned to the carbonatite phases, while the fourth one corresponds to the Si-O stretching vibrations. The small variations in the range of $1000\text{--}1083\text{ cm}^{-1}$ could be attributed to the silicon compounds in the sand [34]. However, the peak at approximately 1083 cm^{-1} is common to both silicates and aragonite, due to the Si-O asymmetric stretching vibrations and the symmetric CO_3 stretching, respectively [35]. The peaks at approximately 470 and 780 cm^{-1} could be ascribed to the silicates [36].

3.2. Mechanical Properties

It is known that the values of compressive strength can vary in a wide range, depending on both the composition and type of mortar. For lime mortars, the compressive strength lies between 0.1 and 1.0 N/mm^2 [37].

The results obtained from the compressive tests in our study are presented in Table 3. As shown in Figure 2, the highest value of compression tensile strength was obtained by the reference mortar, followed by the mortar containing 1% GO. The lowest compression strength was observed in the mortar sample containing ZnO and TiO₂. The statistical Anova test revealed significant differences among the five groups of samples. However, the compressive strength values obtained from the samples M-GO-5%, M-GO-Ag-GO-Fly ash and M-GO-ZnO-GO-TiO₂ are rather similar.

Table 3. Compression test results (following the Tukey test: groups of specimens marked with the same letter show no statistically significant differences between them; the groups marked with different letters show statistically significant differences between them).

Mortar Sample	Load at Break (N) \pm SD	Tensile Strength (MPa) \pm SD
M	124.53 \pm 45.88 ^a	0.59212 \pm 0.17312 ^a
M-GO-1%	193.82 \pm 38.99 ^b	0.49614 \pm 0.12067 ^b
M-GO-5%	162.28 \pm 35.04 ^c	0.40569 \pm 0.10982 ^c
M-GO-Ag-GO-Fly ash	164.03 \pm 29.44 ^d	0.41197 \pm 0.05225 ^c
M-GO-ZnO-GO-TiO ₂	138.38 \pm 31.85 ^e	0.38596 \pm 0.12874 ^c
<i>p</i> value	2.50748 $\times 10^{-7}$	2.43666 $\times 10^{-9}$

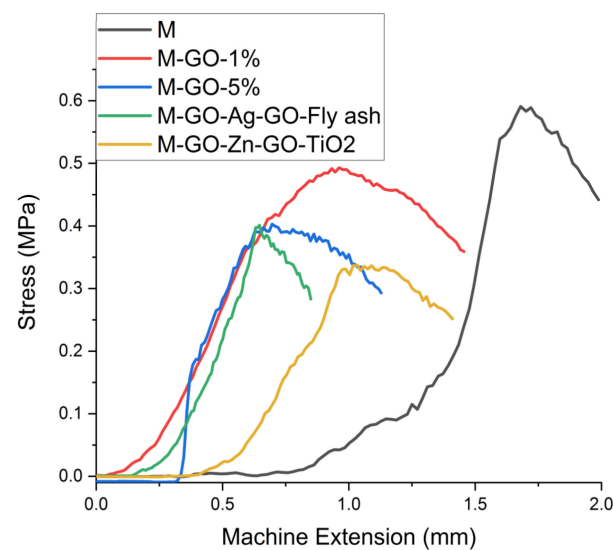


Figure 2. Stress–strain curves in the compression test of the mortars.

The values of the flexural strength presented in Table 4 suggest that the tested mortars present rather weak mechanical characteristics, but these results are consistent with the mechanical properties of the lime mortars generally used in restoration and conservation works. However, the values of the flexural strength from Figure 3 are higher compared to previously reported data for different restoration mortars [34].

Table 4. Flexural test results (following the Tukey test: groups of specimens marked with the same letter show no statistically significant differences between them; the groups marked with different letters show statistically significant differences between them).

Mortar Sample	Load at Maximum Load (N) \pm SD	Maximum Bending Stress (MPa) \pm SD	Load at Break (N) \pm SD
M	131.41 \pm 33.28 ^a	0.37098 \pm 0.05844 ^a	105.12 \pm 20.65 ^a
M-GO-1%	146.14 \pm 25.79 ^b	0.33599 \pm 0.09508 ^b	120.91 \pm 28.63 ^b
M-GO-5%	151.59 \pm 20.95 ^b	0.35528 \pm 0.08038 ^c	121.27 \pm 23.92 ^b
M-GO-Ag-GO-Fly ash	149.95 \pm 23.92 ^b	0.37572 \pm 0.09558 ^d	119.96 \pm 30.86 ^b
M-GO-ZnO-GO-TiO ₂	198.29 \pm 16.04 ^c	0.33238 \pm 0.10195 ^e	158.64 \pm 24.55 ^c
<i>p</i> value	6.08071 $\times 10^{-7}$	6.83773 $\times 10^{-6}$	6.57792 $\times 10^{-7}$

It is known that flexural strength values are affected by the size of the inner pores of the mortar samples, which may contain water that weakens the strength of these materials. In our study, the highest flexural strength was obtained by the Fly ash-containing mortar

sample (see Table 4). From the results obtained, the ductility character of the mortar can be observed. The force required to deform the specimen begins to increase during the test, up to the maximum point of the stress–strain curve which corresponds to the load at maximum load value. The action of this value is the formation of the “neck” specimen, which is accentuated reasonably quickly because the deformation continues to occur only in the neck area with lower forces (because this section of the specimen decreases continuously). Thus, the specimen breaks at load at break value, which corresponds to the point where the material failed.

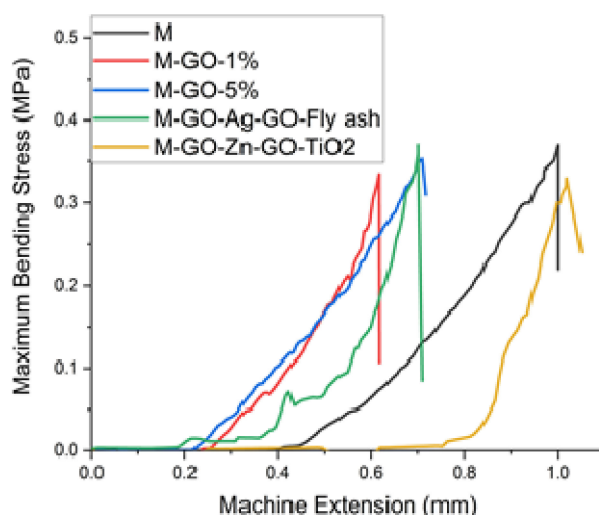


Figure 3. Stress–strain curves in the flexural test of the mortars.

Following the Anova test, statistically significant differences were found among all the tested mortars. However, no significant differences regarding the maximum bending stress were observed among the mortar samples containing GO (M-GO-1% and M-GO-5%) or a mixture of GO-Ag and GO-Fly ash (M-GO-Ag-GO-Fly ash).

According to [38], the mechanical properties of the construction materials depend on the thickness of the tested layer, i.e., the value of the compressive strength increases quickly when the thickness of the mortar layer falls below 25 mm, while the maximum strength is usually obtained for thicknesses corresponding to the normal thickness of the horizontal joints (about 10 ÷ 12 mm).

In our study, the thickness of the layer of the mortars was 40 mm, and the results of the mechanical tests lay within the middle of the accepted ranges for lime mortars (0.1–1.0 N/mm²). The values obtained for the compressive and flexural strengths suggest that the mortars tested present rather poor mechanical characteristics, but they are able to ensure compatibility with the mechanical properties of the bricks to which these mortars are addressed.

In 2017, Faria [34] investigated for the first time the incorporation of GO (in percentages of 0.05%, 0.1%, 0.5%, and 1%) on natural hydraulic lime mortars, determined by the demand to improve the properties of traditional materials used in the rehabilitation of heritage buildings. If, for small percentages of GO additions, the results of flexural strength were maintained and, for compression strength, were slightly higher compared to the reference mortar for larger GO additions, the flexural strength is slightly reduced while the compressive strength increases.

In our study, minor variations were observed in the mechanical properties that decrease by increasing the amount of GO but which show a maximum supported force and a breaking strength greater than the reference mortar, a sign that their ductility increases. Thus, although the overall improvement is not remarkable, the fact that the mechanical strength does not change much allows these mortars to maintain compatibility with historical materials, for applications such as replacing plasters or preserving and repairing

historic buildings where low mechanical properties are required, so these results can be seen to be positive.

Figure 4 shows the results of the adhesive strength of the mortars determined with the pull-off method. Three types of fractures occurred within all tested mortars. The lowest values were obtained from the mortar—adhesive interface fracture (Figure 4c); therefore, they were eliminated from the applied statistical analysis.

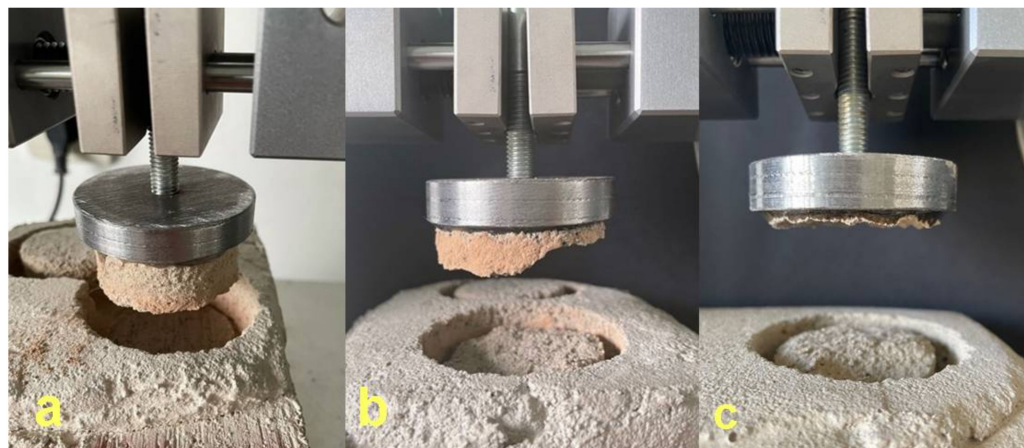


Figure 4. Types of fractures obtained during the adhesion test. (a) Fracture at the interface between the mortar and the brick; (b) Fracture inside the mortar layer; (c) Fracture at the interface between the mortar and the adhesive.

The presence of the fracture at the mortar—brick interface (Figure 4a) correlates with a higher hardness of the tested mortar, compared to the fracture occurring inside the mortar layer (Figure 4b). This appears when the mortar presents a higher adhesion strength in the pores of the support material.

Also known as peak load, the load at maximum load is the maximum load produced during an impact test. Quite often, this point may also correspond to the onset of material damage or complete failure. As shown in Table 5, the addition of GO leads only to slight improvements in the adhesion strength of the brick substrate compared to the reference mortar. Instead, the calculated value of the adhesion strength for the mortar sample incorporating the mixture of GO-Ag and GO-Fly ash is two times higher compared to the reference mortar (Table 5).

Table 5. Adhesive strength of the mortars (following the Tukey test: groups of specimens marked with the same letter show no statistically significant differences between them; the groups marked with different letters show statistically significant differences between them).

Mortar Sample	Load at Maximum Load (N) \pm SD	Tensile Strength (MPa) \pm SD
M	120.10 \pm 20.95 ^a	0.10388 \pm 0.03115 ^a
M-GO-1%	170.98 \pm 18.24 ^b	0.11245 \pm 0.02877 ^a
M-GO-5%	143.12 \pm 10.66 ^c	0.11405 \pm 0.01609 ^a
M-GO-Ag-GO-Fly ash	200.5 \pm 25.81 ^d	0.23512 \pm 0.09959 ^b
M-GO-ZnO-GO-TiO ₂	210.67 \pm 19.05 ^e	0.17143 \pm 0.05132 ^c
<i>p</i> value	6.65134 \times 10 ⁻⁸	3.47601 \times 10 ⁻⁶

Although some significant statistical differences among the five mortar samples were obtained with regard to their adhesion resistance, the Tukey test emphasized that these differences are not important in the case of the reference (M) and GO-containing mortars (M-GO 1% and M-GO 5%).

The results of the adhesive strength tests showed that the mortars containing 5 wt.% GO and the combination of GO-Ag and GO-Fly ash present better adhesion strengths (0.23 MPa) compared to the reference mortar sample (0.10 MPa) (Figure 5). Moreover, in the case of the M-GO-Ag-GO-Fly sample, the pull-off test revealed that more fractures occur in the mortar layer than at the mortar—brick interface.

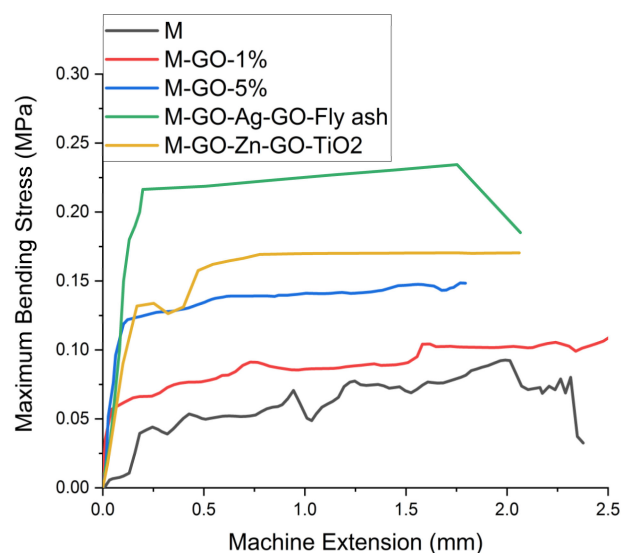


Figure 5. Push-off test.

3.3. Morphological and Structural Characterization

The SEM images obtained on the mortar surfaces are shown in Figure 6.

Despite their homogeneous composition, the surface texture of the five mortars showed visible differences, as illustrated in Figure 6. Thus, the reference mortar (Figure 6a–c) presented a high porosity within the carbonate matrix, in which two types of crystalline growth emerged, i.e., with large and small particles. Instead, good internal cohesion between the components of the mortars containing GO and various additives was observed in Figure 6d–o.

Taking into account that the only difference between the five samples is related to the addition of some minor components, it could be asserted that the adhesion between the matrix and the aggregate is influenced not only by the texture of the aggregate particles, the presence of the GO-based added combinations and the nature and texture of these nanoparticles, but also by the viscosity of the mixture and the superficial tension [39].

3.4. Surface Deterioration of the Mortars Exposed to Chemical Attack

In an attempt to evaluate the behavior of the mortars in various corrosive environments, the reference mortar (M) and the mortar specimen presenting the best mechanical properties (M-GO-Ag-GO-Fly ash) were further subjected to chemical attacks. The surfaces of the mortars after exposure to the chemicals were examined using SEM, and the results are shown in Figure 7.

The attack of the nitric acid on the mortar matrix leads to the formation of calcium nitrate, which is a very soluble salt [40]. As a result, insoluble precipitates surrounding the areas of the unaffected material are formed. Consequently, variations of the pH in the degraded surface layer are expected, from very low values due to the acidic solution being in contact with the mortar, to high alkaline values that are characteristic of the unaffected material. The formed precipitates are soft, very porous, and present cracks on the surface caused by contractions during decalcification [40].

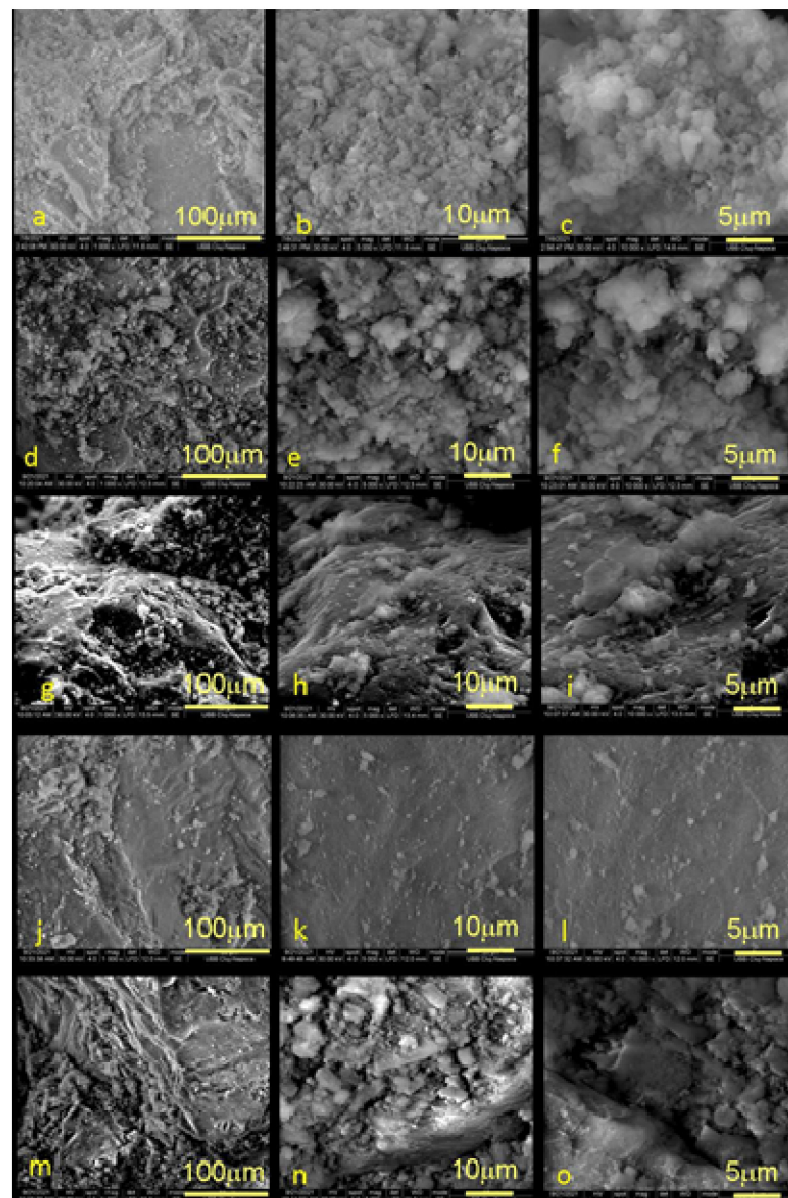


Figure 6. SEM images showing the morphology of the surfaces of the tested mortars: (a–c) Reference mortar (M); (d–f) M-1% GO; (g–i) M-5% GO; (j–l) M-GO-Ag-GO-Fly ash; (m–o) M-GO-ZnO-TiO₂.

The corrosive substances can create cracks in the surface layer of the mortar, and cause material failure over time. Hence, for this type of construction material, the most important issue is the observation of a ‘neutral’ behavior to chemical attacks on the surface. As seen in Figure 7, a greater particle release from the surface layer of the tested mortar takes place, as the pH of the corrosive solutions decreases. The most degraded surface areas were noticed for the mortars in contact with the mixture of sulfuric acid and nitric acid (Figure 7c,f) and with the acetic acid solution (Figure 7b,e).

The results of the adhesive strength tests showed that the mortars containing 5 wt.% GO and the combination of GO-Ag and GO-Fly ash present better adhesion strengths (0.23 MPa) compared to the reference mortar sample (0.10 MPa). Moreover, in the case of the M-GO-Ag-GO-Fly sample, the pull-off test revealed that more fractures occur in the mortar layer than at the mortar–brick interface.

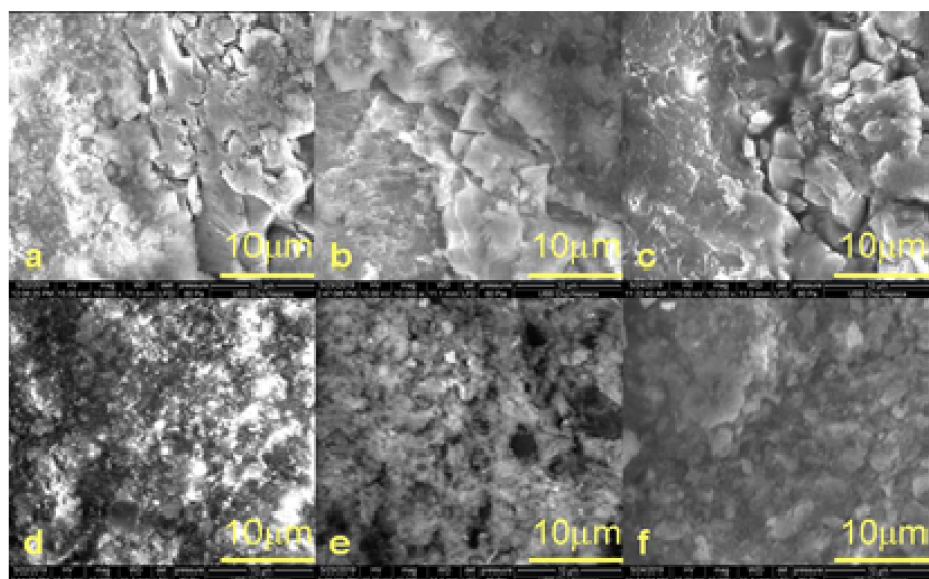


Figure 7. SEM images of the mortar surface after exposure to various corrosive solutions: (a,d) Rain-water (pH = 6); (b,e) Acetic acid (pH = 3.5); (c,f) Sulfuric and nitric acid (pH = 2). (a–c) Reference mortar (M); (d–f) GO-Ag-GO-Fly ash.

It was reported [34] that the addition of well-dispersed GO (0.01–0.06% by weight) and other various nanoparticles could improve the strength and durability of cements and mortars due to their filler effect, because smaller particles can easily penetrate spaces created by the joining of larger particles [34]. Particularly, GO possesses hydroxyl (–OH), epoxy (–CH(O)CH–), carboxyl (–COOH), and carbonyl (–C=O) groups that are attached to the surface and to the edges of its sheets, which assist their effective dispersion in the water, due to electrostatic stabilization. Likewise, the addition of GO in the cement matrix reduces the need of using surfactants, which are commonly added to prevent the nanomaterials agglomeration caused by van der Waals attractive forces. Nonetheless, the carboxyl groups of GO are able to interact with the cement hydrates, creating a 3D network structure in the cementitious matrix [41], which could minimize the acid attack on the material surface.

The lifespan of mortar structures depends mainly on the durability of the substrate to which it is attached, and their durability is directly related to the presence of water due to their increased porosity.

4. Conclusions

In the present paper, several mortars incorporating graphene oxide without and with different mixtures of functionalized additives (Ag, Fly ash, ZnO and TiO₂) were prepared. Various mechanical, physico-chemical, and microscopical tests were carried out to evaluate the durability and mechanical properties of the natural lime mortar composites that were intended to be further used in cultural heritage restoration processes.

The results obtained showed that the compressive and flexural strengths of the mortars incorporating nanomaterials are reduced compared to the reference sample, while their adhesion strength to the brick substrate increased. The best results were obtained by incorporating a mixture of GO-Ag and GO-Fly ash into the reference mortar sample. The M- GO-Ag and GO-Fly ash also showed good resistance to chemical attacks.

Author Contributions: Conceptualization, P.D. (Popa Dorin) and P.D. (Prodan Doina); methodology, M.M.; software, S.C.; validation, V.S., P.M.; formal analysis, I.R.; investigation, C.S.; resources, M.M.; data curation, E.R.; writing—original draft preparation, C.S.; writing—review and editing, V.S.; visualization, E.R.; supervision, S.C. All authors have read and agreed to the published version of the manuscript.

Funding: The research received no external funding.

Institutional Review Board Statement: Not applicable.

Informed Consent Statement: Not applicable.

Data Availability Statement: Not applicable.

Acknowledgments: This work was supported by a grant from the Romanian Ministry of Education and Research, CCCDI—UEFISCDI, project number PN-III-P2-2.1-PED-2019-3739, no. 565 PED/2020.

Conflicts of Interest: The authors declare no conflict of interest.

References

1. Haach, V.G.; Vasconcelos, G.; Lourenco, P.B. Influence of aggregates grading and water/cement ratio in workability and hardened properties of mortars. *Constr. Build. Mater.* **2011**, *25*, 2980–2987. [[CrossRef](#)]
2. Coppola, L.; Coffetti, D.; Crotti, E. Plain and ultrafine fly ashes mortars for environmentally friendly construction materials. *Sustainability* **2018**, *10*, 874. [[CrossRef](#)]
3. Venkatarama Reddy, B.V.; Gupta, A. Influence of sand grading on the characteristics of mortars and soil–cement block masonry. *Constr. Build. Mater.* **2008**, *22*, 1614–1623. [[CrossRef](#)]
4. Apostolopoulou, M.; Armaghani, D.J.; Bakolas, A.; Douvikas, M.G.; Moropoulou, A.; Asteris, P.G. Compressive strength of natural hydraulic lime mortars using soft computing techniques. *Procedia Struct. Integr.* **2019**, *17*, 914–923. [[CrossRef](#)]
5. Bauer, E.; Silva, E.F.; Sousa, J.G.G.; Salomao, M.C.F. Friction influence between particles in the behavior of flow of lime-rendering mortars. *J. Mater. Civil. Eng.* **2015**, *27*, 04014136. [[CrossRef](#)]
6. Meng, T.; Yu, Y.; Qian, X.; Zhan, S.; Qian, K. Effect of nano-TiO₂ on the mechanical properties of cement mortar. *Constr. Build. Mater.* **2012**, *29*, 241–245. [[CrossRef](#)]
7. Casagrande, C.A.; Jochem, L.F.; Repette, W.L.; Hotza, D. Evaluation of nano-TiO₂ on properties of cementitious mortars. *Matéria* **2020**, *25*, 12883. [[CrossRef](#)]
8. Prodan, D.; Moldovan, M.; Furtos, G.; Saroși, C.; Filip, M.; Perhaita, I.; Carpa, R.; Popa, M.; Cuc, S.; Varvara, S.; et al. Synthesis and characterization of some graphene oxide powders intended to improve the quality of hydraulic mortars. *Appl. Sci.* **2021**, *11*, 11330. [[CrossRef](#)]
9. Emiru, T.F.; Ayele, D.W. Controlled synthesis, characterization and reduction of graphene oxide: A convenient method for large scale production. *Egypt. J. Basic Appl. Sci.* **2017**, *4*, 74–79. [[CrossRef](#)]
10. Lu, Z.Y.; Lu, C.; Leung, C.K.Y.; Li, Z. Graphene oxide modified Strain Hardening Cementitious Composites with enhanced mechanical and thermal properties by incorporating ultra-fine phase change materials. *Cem. Concr. Comp.* **2019**, *98*, 83–94. [[CrossRef](#)]
11. Indukuri, C.S.R.; Nerella, R.; Madduru, S.R.C. Effect of graphene oxide on microstructure and strengthened properties of fly ash and silica fume based cement composites. *Constr. Build. Mater.* **2019**, *229*, 116863. [[CrossRef](#)]
12. Liu, C.; Huang, X.; Wu, Y.Y.; Deng, X.; Zheng, Z. The effect of graphene oxide on the mechanical properties, impermeability and corrosion resistance of cement mortar containing mineral admixtures. *Constr. Build. Mater.* **2021**, *288*, 123059. [[CrossRef](#)]
13. Diamantopoulos, G.; Katsioti, M.; Fardis, M.; Karatasios, I.; Alhassan, S.; Karagianni, M.; Papavassiliou, G.; Hassan, J. The role of titanium dioxide on the hydration of portland cement: A combined NMR and Ultrasonic Study Molecules. *Molecules* **2020**, *25*, 5364. [[CrossRef](#)]
14. Sanchez, F.; Sobolev, K. Nanotechnology in concrete—A review. *Constr. Build. Mater.* **2010**, *24*, 2060–2071. [[CrossRef](#)]
15. Rattan, C.S.; Witanun, N.; Nuntawong, N.; Chindaudom, P.; Oaew, S.; Kedkeaw, C.; Limsuwan, P. Preparation and characterization of graphene oxide nanosheets. *Procedia Eng.* **2012**, *32*, 759–764. [[CrossRef](#)]
16. Gao, Y.; Jing, H.; Fu, G.; Zhao, Z.; Shi, X. Studies on combined effects of graphene oxide-fly ash hybrid on the workability, mechanical performance and pore structures of cementitious grouting under high W/C ratio. *Constr. Build. Mater.* **2021**, *281*, 122578. [[CrossRef](#)]
17. Wang, Y.; Yang, J.; Ouyang, D. Effect of graphene oxide on mechanical properties of cement mortar and its strengthening mechanism. *Materials* **2019**, *12*, 3753. [[CrossRef](#)]
18. Cui, D.; Wei, H.; Zuo, X.; Zheng, K.; Wang, Q. Use of graphene oxide to improve the durability and mechanical properties of mortar immersed in flowing river for three years. *Nanomaterials* **2020**, *10*, 2385. [[CrossRef](#)]
19. Hong, X.; Lee, J.C.; Qian, B. Mechanical properties and microstructure of high-strength lightweight concrete incorporating graphene oxide. *Nanomaterials* **2022**, *12*, 833. [[CrossRef](#)]
20. Wang, Q.; Qi, G.; Wang, Y.; Zheng, H.; Shan, S.; Lu, C. Research progress on the effect of graphene oxide on the properties of cement-based composites. *New Carbon Mater.* **2021**, *36*, 729–750. [[CrossRef](#)]
21. Tran, M.H.; Jeong, H.K. Synthesis and Characterization of Silver Nanoparticles Doped Reduced Graphene Oxide. *Chem. Phys. Lett.* **2015**, *630*, 80–85. [[CrossRef](#)]
22. El-Shafai, N.; El-Khouly, M.E.; El-Kemary, M.; Ramadan, M.; Eldesoukey, I.; Masoud, M. Graphene oxide decorated with zinc oxide nanoflower, silver and titanium dioxide nanoparticles: Fabrication, characterization, DNA interaction, and antibacterial activity. *RSC Adv.* **2019**, *7*, 3704–3714. [[CrossRef](#)]

23. Khorrami, S.; Abdollahi, Z.; Eshaghi, G.; Khosravi, A.; Bidram, E.; Zarrabi, A. An improved method for fabrication of Ag-GO nanocomposite with controlled anticancer and antibacterial behavior; A comparative study. *Sci. Rep.* **2019**, *9*, 9167. [[CrossRef](#)] [[PubMed](#)]
24. Baboo, R.; Kumar, S.; Kumar, S. Effect of fly ash on mortat mixes with quarry dust as fine aggregate. *Mat. Sci. Eng.* **2014**, *2014*, 626425. [[CrossRef](#)]
25. Chindapasirt, P.; Jaturapitakkul, C.; Sinsiri, T. Effect of fly ash fineness on compressive strength and pore size of blended cement paste. *Cem. Concr. Compos.* **2005**, *27*, 425–428. [[CrossRef](#)]
26. Oltulu, M.; Şahin, R. Effect of nano-SiO₂, nano-Al₂O₃ and nano-Fe₂O₃ powders on compressive strengths and capillary water absorption of cement mortar containing fly ash: A comparative study. *Energ. Buil.* **2013**, *58*, 292–301. [[CrossRef](#)]
27. Pavia, S.; Treacy, E. A comparative study of the durability and behaviour of fat lime and feebly-hydraulic lime mortars. *Mater. Struct.* **2006**, *39*, 391–398. [[CrossRef](#)]
28. Veiga, M.d.R.; Fragata, A.; Velosa, A.L.; Magalhães, A.C.; Margalha, G. Lime-based mortars: Viability for use as substitution renders in historical buildings. *Inter. J. Archit. Herit.* **2010**, *4*, 177–195. [[CrossRef](#)]
29. *SR EN 1015-11:2002*; Methods of Test for Mortar for Masonry-Part 11: Determination of Flexural and Compressive Strength of Hardened Mortar. Slovenian Institute for Standardization: Ljubljana, Slovenia, 2002.
30. *EN 1607:1996/1607:1997*; Thermal Insulating Products for Building Applications. Determination of Tensile Strength Perpendicular to Faces. Serbian Institute for Standardization: Belgrade, Serbia, 1997.
31. *ASTM C348-14*; Standard Test Method for Flexural Strength of Hydraulic-Cement Motars. ASTM: New York, NY, USA, 2013.
32. *SR EN 1015-12:2001*; Methods of Test for Mortar for Masonry-Part 12: Determination of Adhesive Strength of Hardened Rendering and Plastering Mortars on Substrates. Slovenian Institute for Standardization: Ljubljana, Slovenia, 2001.
33. Brunello, V.; Corti, C.; Sansonetti, A.; Tedeschi, C.; Rampazzi, L. Non-invasive FTIR study of mortar model samples: Comparison among innovative and traditional techniques. *Europ. Physic. J. Plus* **2019**, *134*, 270. [[CrossRef](#)]
34. Faria, P.; Duarte, P.; Barbosa, D.; Ferreira, I. New composite of natural hydraulic lime mortar with graphene oxide. *Constr. Build. Mater.* **2017**, *156*, 1150–1157. [[CrossRef](#)]
35. Diekamp, A.; Stalder, R.; Konzett, J.; Mirwald, P.W. Lime mortar with natural hydraulic components: Characterisation of reaction rims with FTIR Imaging in ATR-mode. *Hist. Mort.* **2012**, *7*, 105–113.
36. Wan, Y.J.; Gong, L.X.; Tang, L.C.; Wu, L.B.; Jiang, J.X. Mechanical properties of epoxy composites filled with silane-functionalized graphene oxide. *Comp. A Appl. Sci. Manuf.* **2014**, *64*, 79–89. [[CrossRef](#)]
37. The Official Monitor of Romania, PART I, Nr. 389 bis/11.VI.2010, Acts of the Specialized Bodies of the Central Public Administration of Regional Development and Tourism, ORDER to Complete the Technical Regulation “Design Code for Masonry Structures”, Indicative CR 6-2006, Approved by Transport Order, Constructions and Tourism no. 1.712/2006 *). 2010, p. 36. Available online: https://www.mdlpa.ro/userfiles/reglementari/Domeniul_V/V_9_2_CR_6_2006_COMPLETARE.pdf (accessed on 6 October 2021).
38. Amrhein, J.E. *Reinforced Masonry Engineering Handbook*, 5th ed.; Updated; Masonry Institute of America: Los Angeles, CA, USA, 1998.
39. Romero-Hermida, M.I.; Borrero-López, A.M.; Flores-Alés, V.; Alejandre, F.J.; Franco, J.M.; Santos, A.; Esquivias, L. Characterization and analysis of the carbonation process of a lime mortar obtained from phosphogypsum waste. *Int. J. Environ. Res. Public Health* **2021**, *18*, 6664. [[CrossRef](#)]
40. Muthu, M.; Santhanam, M. Effect of reduced graphene oxide, alumina and silica nanoparticles on the deterioration characteristics of Portland cement paste exposed to acidic environment. *Cem. Conc. Compos.* **2018**, *91*, 118–137. [[CrossRef](#)]
41. Wang, M.; Wang, R.; Yao, H.; Farhan, S.; Zheng, S.; Du, C. Study on the three dimensional mechanism of graphene oxide nanosheets modified cement. *Construct. Build. Mater.* **2016**, *126*, 730–739. [[CrossRef](#)]